

Shape Transition in the Even-Even Cerium Isotopes

Benyoucef Mohammed-Azizi¹, Abderrachid Helmaoui², and Djamel-Eddine Medjadi³

¹University of Bechar, Bechar, Algeria. E-mail: azizyoucef@voila.fr

²University of Bechar, Bechar, Algeria. E-mail: helmaouiabderrachid@yahoo.fr

³École Normale Supérieure, Vieux Kouba, Algiers, Algeria. E-mail: medjadide@voila.fr

The deformation energy of the even-even nuclei of the Cerium isotopic chain is investigated by means of the Macroscopic-Microscopic method with a semiclassical shell correction. We consider axially symmetric shapes. Binding energy and two neutron separation energy are also evaluated. For the sake of clarity several important details of the calculations are also given. It turns out that all these nuclei have prolate equilibrium shape. The regions of maximum deformation are obtained around $N = 64$ and $N = 102$. There is no critical-point of quantum phase transition in this isotopic chain.

1 Introduction

Nowadays it is well established that the majority of nuclei possess a nonzero intrinsic electric quadrupole moment (IE QM). This feature means that the charge distribution inside the nucleus deviates from the spherical symmetry. In other words, apart from very few nuclei, the surface of the nucleus is generally not spherical in its ground state. The intrinsic quadrupole electric moments (or equivalently the nuclear deformation) can be deduced from two types of measurements:

- The reduced electric quadrupole transition probability, $B(E2)$ [1];
- The static electric quadrupole moments of ground and excited states, Q [2].

It turns out that in a number of cases, the two methods of measurement do not systematically lead to the same values. Important discrepancies occur for several nuclei. This is essentially due to the fact that not only different experimental techniques are used but above all, because different models can be implemented to deduce the nuclear deformation for the both cases.

In [3] it is stated that deformations deduced from $B(E2)$ have a “more general character”. In other words, “ $B(E2)$ -type” data reflect not only static nuclear deformation (permanent deviation of the nuclear shape from sphericity), but also dynamic deformation. Furthermore, $B(E2)$ measurements are model independent and thus are generally more reliable. This is corroborated by the fact that the only systematic compilation in which the deformation of the ground state is given explicitly is based on $B(E2; 0^+ \rightarrow 2^+)$ and has been published in [1]. In the present work, experimental values refer to these ones.

Theoretical approaches to the deformation energy can be divided into two categories; Dynamic calculations to find the shape of the ground state (or even of excited states) and static calculations by determining the absolute minimum (ground state) or multiple minima (shape isomers) in the potential energy surface (PES) for a given nucleus.

Thus, on the one hand, we have the so-called collective models, which themselves are subdivided into two groups: The “Geometric Collective Model” also called the “Collective Bohr Hamiltonian” (CBH and its variants) and the “Algebraic Model”, well known under the name of the “Interacting Boson Model” (IBM and its variants) [4]. On the other hand, “particle models” consider the nucleus as a collection of interacting nucleons (fermions).

In practice, the classical N -body problem can be approximately solved by the usual approximation of the mean field with eventually residual interactions. In this respect, the “best” mean field is deduced after applying a variational principle in the Hartree-Fock-Bogoliubov method (HFB). In this model, the determination of the potential energy surface (PE S) of the nucleus amounts to perform constrained Hartree-Fock-Bogoliubov (CHF B) calculations [5]. We will not address very complicated methods “beyond the mean field” such as the Quasiparticle Random Phase Approximation (QRPA) or the Generator-Coordinate-Method (GCM) methods which are unsuitable in practice for large scale calculations.

Because of CHF B calculations are time consumers, especially in large studies, Microscopic-Macroscopic method (Mic-Mac) constitutes a good alternative which, is up to now, implemented [6]. In the present work, we use an improved variant of this method. The word “improved” means that we use semi-classical method to avoid the well-known drawbacks (spurious dependence on two mathematical parameters) of the standard Strutinsky shell correction (see text below).

The present study is devoted to the deformation energy, equilibrium nuclear shapes and binding energy of the ground state of the even-even cerium isotopes. There are many reasons to this choice. One of them is to re-test our previous calculations. In effect, similar calculations have been already performed by us in the xenon, barium, and cerium region [7]. However because the phenomenological mean potential varies smoothly with N and Z , we have made, in the past, a rough approximation by choosing the same set of parameters for the phenomenological mean potential, for the all treated

nuclei. Originally, this approximation was done only for simplifying the calculations.

Here, contrarily to that study, each nucleus has its “own” mean potential with a specific set of parameters. In this way it is possible to evaluate in a rigorous way the uncertainty introduced in the previous calculations. Apart from this remark, there are several main other reasons which could justify this choice: (i) First, it should be interesting to see how the deformation energy and binding energy vary with the neutron number (N) for this isotopic chain. (ii) Second, the present study extends the previous calculations to all cerium isotopes up to the drip lines (34 versus 13 nuclei). (iii) Third, we also will attempt to deduce, from potential energy surface (PES) curves, the shape transition from spherical to axially deformed nuclei, looking for the so-called $X(5)$ critical-point between $U(5)$ and $SU(3)$ symmetry limits of the IBM [8, 9].

It is worth to recall briefly some information deduced from the literature for the cerium isotopes. In the past, a number of experimental as well as theoretical studies have been done for the cerium isotopes. Among the numerous studies, we only cite some of them.

In 2005 Smith et al [10] have studied excited states of ^{122}Ce up to spin $14\hbar$ deducing a probable quadrupole deformation of about $\beta \approx 0.35$. The deformed nucleus ^{130}Ce has been studied in 1985, using the techniques of in-beam gamma-ray spectroscopy [11]. The corresponding data have been interpreted in terms of the cranking model by assuming a prolate deformation with $\varepsilon_2 \approx 0.25$ ($\beta \approx 0.27$).

High-spin states in ^{132}Ce have been also studied by A.J. Kirwan et al [12]. They found a superdeformed band with deformation $\beta \approx 0.4$ much more larger than the ground state deformation ($\beta \approx 0.2$). E. Michelakakis et al [13] by evaluating γ -ray transitions in ^{142}Ce and ^{144}Ce conclude that in cerium isotopes (near the beta-stable line) the onset of nuclear deformation occur between $N = 86$ and $N = 88$. “Pure” theoretical calculations have been performed in [14] and [15] with projected shell model (PSM) and Hartree-Bogoliubov ansatz in the valence space respectively for ^{122}Ce and $^{124-132}\text{Ce}$ for low lying yrast spectra. Good values of energy levels and reduced transition probabilities $B(E2, 0^+ \rightarrow 2^+)$ have been obtained respectively in these two papers.

Other approaches for the rich-neutron cerium isotopes have been made in [16]. A study of the shape transition from spherical to axially deformed nuclei in the even Ce isotopes has been done in [17] using the nucleon-pair approximation of the shell model. The result of a such study is that the transition has been found too rapid. Relativistic Hartree-Fock-Bogoliubov theory has been used to predict ordinary halo for ^{186}Ce , ^{188}Ce , ^{190}Ce , and giant halo for ^{192}Ce , ^{194}Ce , ^{196}Ce , and ^{198}Ce near the neutron drip line.

Systematic studies about nuclear deformations and masses of the ground state can be found in [18–21] with respectively, the Finite-Range Droplet-Model (FRDM), Hartree-Fock-Bogoliubov (HFB), HFB+5-dimensional collective qua-

drupole Hamiltonian and Relativistic Mean Field (RMF) models.

2 The Macroscopic–Microscopic method

2.1 Liquid drop model and microscopic corrections

This method combines the so-called semi-empirical mass formula (or liquid drop model) with shell and pairing corrections deduced from microscopic model. Thus the binding energy is given as a function of nucleon numbers and deformation parameter (referred to as β) by mean of the usual symbols:

$$B(A, Z, \beta) = E_{LDM}(\beta) - \delta B_{micro}(\beta). \quad (1)$$

δB_{micro} contains the shell and pairing correction (see text below). The minus sign before δB_{micro} is consistent with the convention that the binding energy is defined as positive here.

For the liquid drop model we take the old version of Myers and Swiatecki [28] (because of its simplicity compared to more recent formulae). Here, there is no need to look for very high accuracy in binding energy, because this is not the purpose of the present work.

$$E_{LDM}(\beta) = C_V A - C_S A^{2/3} B_S(\beta) - C_C Z^2 A^{-1/3} B_C(\beta) + \varepsilon a_{pair} A^{-1/2} + C_d Z^2 A^{-1}. \quad (2)$$

In (2), we have the usual contributions of volume, surface and coulomb energies.

The different constants of Myers and Swiatecki are given in Appendix A. The shape dependence (β) of the surface and coulomb energies are contained in $B_S(\beta)$ and $B_C(\beta)$. They are normalized to the unity for a spherical nuclear surface. The latter is symbolized by $\beta = 0$. The two last terms in (2) are respectively due to the smooth part of the pairing energy and the correction of the Coulomb energy to account for the diffuseness of the nucleus surface. The different constants will be fixed later.

The potential energy surface (PES without zero point energy correction) is defined as follows:

$$E_{PES}(\beta) = E_{LDM}(0) - B(A, Z, \beta) = \Delta E_{LDM}(\beta) + \delta B_{micro}(\beta) \quad (3)$$

in which

$$\Delta E_{LDM}(\beta) = E_{LDM}(0) - E_{LDM}(\beta) = C_S A^{2/3} [B_S(\beta) - B_S(0)] + C_C Z^2 A^{-1/3} [B_C(\beta) - B_C(0)]. \quad (4)$$

Constants C_V and C_S are expressed by means of three other constants a_V , a_S , and κ . For spherical shape, as said before, the normalization is expressed by: $B_S(0) = B_C(0) = 1$. As it can be easily seen, the potential energy surface is related only to two macroscopic constants C_S (which depends actually on

a_S and κ) and C_C . To calculate microscopic shell and pairing corrections contained in δB_{micro} , we have to proceed in two steps. The first consists in solving the Schrödinger equation and the second in deducing the shell and pairing corrections in an appropriate way, as explained in the following.

2.2 Microscopic model

We briefly present the microscopic model which is based on the Schrödinger equation of the deformed independent particle model:

$$\hat{H}(\beta) | \Psi_i(\beta) \rangle = \varepsilon_i(\beta) | \Psi_i(\beta) \rangle \quad (5)$$

where $|\Psi_i\rangle$ and ε_i are respectively the eigenfunctions and the associated eigenvalues of nucleons. Hamiltonian \hat{H} contains four contributions which are: (i) kinetic energy, (ii) central deformed mean field, (iii) spin-orbit and (iv) Coulomb interactions.

We perform analogous calculations as in Nilsson model but our deformed mean potential is of Woods-Saxon type and therefore is “more realistic”. Although calculations are not self consistent, they are microscopic. It is to be noted that our Schrödinger equation has a form which is very close to the one of the Skyrme-Hartree-Fock method. Eq. (5) is solved by our FORTRAN program described in details in [22] and improved in two successive versions [23] and [24].

2.3 Microscopic corrections

Microscopic corrections are defined as the sum of shell and pairing corrections which themselves are calculated separately for each kind of nucleons:

$$\begin{aligned} \delta B_{micro}(\beta) = & \delta E_{shell}(N, \beta) + \delta E_{shell}(Z, \beta) + \\ & + \delta P_{pairing}(N, \beta) + \delta P_{pairing}(Z, \beta). \end{aligned} \quad (6)$$

In this formula the shell correction is defined by the usual Strutinsky prescription, i.e. as the difference between the sum of the single particle energies (which contains the shell effects) and an averaged (or smoothed) sum (which is free from shell effects)

$$\delta E_{shell}(N \text{ or } Z) = \sum_{i=1}^{N \text{ or } Z} \varepsilon_i(\beta) - \overline{\sum_{i=1} \varepsilon_i(\beta)}. \quad (7)$$

Energies $\varepsilon_i(\beta)$ are deduced from (5). In our procedure, the second sum is found by means of a semi-classical way instead a Strutinsky smoothing procedure, see [27]. This avoids the well-known weakness of the standard shell correction method, namely, the dependence on two unphysical parameters which are the “smoothing” parameter and the order of the curvature correction.

Moreover, it has been clearly shown that Strutinsky level density method is only an approximation of that of the semi-classical theory [26]. The “pure” pairing correlation energy

is defined by:

$$P(\beta) = \sum_{i=1}^{\infty} 2\varepsilon_i(\beta)v_i^2 - \sum_{i=1}^{N/2 \text{ or } Z/2} 2\varepsilon_i(\beta) - \frac{\Delta^2}{G} \quad (8)$$

where v_i^2 , Δ and λ are the usual occupation probabilities, gap and Fermi energy of the BCS approximation (the factor “2” is simply due to the Kramers degeneracy). Since the smooth part of pairing correlations is already contained in the liquid drop model, we have to add only the one due to the shell oscillations of the level density. This contribution is defined by means of a formula similar to (7)

$$\delta P_{pairing}(N \text{ or } Z, \beta) = P(\beta) - \overline{P(\beta)} \quad (9)$$

where the averaged pairing is defined as

$$\overline{P(\beta)} = \frac{1}{2} g_{semicl.}(\lambda) \overline{\Delta}^2.$$

We use a simple BCS method to account for pairing correlations. To calculate (7) and (9) we follow the method detailed in [27] with its FORTRAN code. The treatment of the pairing has also been explained in [7] and references quoted therein.

2.4 Numerical constants and prescriptions

2.4.1 Constants of the microscopic model

For each kind of particles the mean central and the mean spin-orbit field are written as [22]:

$$\begin{aligned} V(\beta) &= \frac{V_0}{1 + \exp(R_V L_V(\beta)/a_0)} \\ V_{SO}(\beta) &= \lambda \left(\frac{\hbar}{2Mc} \right) \frac{V_0}{1 + \exp(R_{SO} L_{SO}(\beta)/a_0)} \end{aligned} \quad (10)$$

where $L_V(\beta)$ and $L_{SO}(\beta)$ contain the information on the deformation. In fact, these functions contain 9 constants: V_{0neut} , V_{0prot} , R_{Vneut} , R_{Vprot} , $R_{SO-neut}$, $R_{SO-prot}$, a_0 , λ_{neut} , λ_{prot} . These quantities are taken from the “universal” parameters [29] (see Appendix B) which is an optimized set. The Coulomb mean field is approximated by a uniform charge distribution inside a deformed surface. The volume conservation is therefore $Vol = (4/3)\pi R_{ch}^3$ with the simple assumption $R_{ch} = R_{Vprot}$.

2.4.2 Constants of the liquid drop model

As already stated, we have chosen the parameters of Myers and Swiatecki (see Table 1) because this set contains a reduced number of parameters with respect to more modern formulae. All the constants are needed in the binding energy whereas only a_S , C_C , κ play a role in the potential energy surface.

	a_V	a_S	C_C	κ	C_d	a_{pair}
Myers and Swiatecki	15.67 MeV	18.56 MeV	0.72 MeV	1.79	1.21 MeV	11 MeV

Table 1: Parameters of the liquid drop model in the Myers and Swiatecki version [28].

2.4.3 Nuclear mass excesses

Nuclear masses are deduced as mass excesses:

$$M_{excess}(A, Z) = ZM_H + (A - Z)M_n - B(A, Z)$$

where $M_H = 7.289034$ MeV is the hydrogen mass excess and $M_n = 8.071431$ MeV the neutron mass excess. This makes comparisons with experimental values easiest.

3 Results

In our previous paper [7] calculations for isotopes $^{116-130}\text{Ce}$ showed that the equilibrium deformations ($\beta \approx 0.25 - 0.30$) have always been obtained for symmetric prolate shapes ($\gamma = 0^\circ$). Results obtained in [32] with a similar approach for the nuclei $^{116-130}\text{Ce}$, corroborate this fact. For these reasons, we think that it is needless to account for the axial asymmetry in a “pure” static study of the equilibrium deformation. However, we have to consider prolate ($\gamma = 0^\circ$) as well as oblate ($\gamma = 60^\circ$) nuclear shapes. In this regard, it is worth remembering that oblate shape given by ($\beta > 0, \gamma = 60^\circ$) is equivalent to the set ($\beta < 0, \gamma = 0^\circ$).

3.1 Comparison between the different contributions entering in the potential energy surface

It could be useful to compare the importance of the different terms entering in the right hand side of (6). In this respect, we have drawn in Fig.1 for axially prolate shape, the four microscopic contributions

$$\delta E_{shell}(N, \beta), \delta E_{shell}(Z, \beta), \delta P_{pairing}(N, \beta), \delta P_{pairing}(Z, \beta)$$

for the case of ^{160}Ce as functions of β . Following the cited order, we can say that the difference between the highest and lowest values in the interval $\beta \in [0.0, 0.7]$ are respectively about 11.0 MeV, 10.5 MeV, 5.7 MeV, 3.5 MeV for the four corrections.

Thus, these variations show that the shell corrections

$$\delta E_{shell}(N, \beta), \delta E_{shell}(Z, \beta)$$

are more important than

$$\delta P_{pairing}(N, \beta), \delta P_{pairing}(Z, \beta)$$

and have a clear minimum at respectively $\beta = 0.35$ and $\beta = 0.30$. It is well known that for each kind of nucleon the shell correction is in opposite phase with respect to the pairing correction (this means for that when $\delta E_{shell}(N, \beta)$ increases with β , $\delta P_{pairing}(N, \beta)$ decreases and vice versa).

Contrarily to these curves, the liquid drop model is strictly increasing with β , and its minimum occurs always at the beginning $\beta = 0.0$ (spherical shape). When all the contributions are added, the minimum of the potential energy surface of the nucleus is reached at about $\beta = 0.3$ and is mainly due to the shell corrections. When β becomes more and more, larger the contribution of the liquid drop energy becomes preponderant so that the equilibrium deformation occurs generally between $\beta = 0$ and $\beta = 0.4$. Because of the convention of the sign stated before, δB_{micro} defined in (1) must be negative in order to increase the binding energy of the nucleus. Since the shell corrections (for protons and neutrons) play a major role in δB_{micro} , it is naturally expected that negative (but absolute large) values of shell correction contribute to increase the binding energy of the nucleus.

In this respect, it is well known that the shell correction is essentially determined by the distribution of single-particle levels in the vicinity of the sharp Fermi level (defined here as midway between the last occupied level and the first empty level). Following [31], we can state that “the nuclear ground state, as well as any other relatively stable state, should correspond to the lowest possible degeneracy, or, in other words, the lowest density of state near the Fermi level”. This is illustrated in Fig. 2 where the single-particle levels are drawn as function of the deformation β (γ being fixed at $\gamma = 0^\circ$). To this end we have used the FORTRAN code of [22] and [24]. The area where the single-particle level density is low near the Fermi level (black stars) is indicated by a circle. Thus, it is not so surprising that, it is in this region where the neutron shell correction becomes the most important, involving a minimum in the PES of the nucleus.

3.2 Equilibrium deformations

Equilibrium deformations are given in Table (2) for prolate as well as oblate shapes (see table legend for details). The minima of PES for the corresponding wells are denoted *minpro* and *minobl*. The deformation energy is defined as the difference $E_{def} = E_{PES}(0) - E_{PES}^{min}(\beta)$, i.e. the difference between the potential energy surface for a spherical shape and the one corresponding to the absolute minimum of PES. Permanent deformations will be in principle characterized by large values of E_{def} and are responsible of rotational spectra.

From this table, some remarks may be drawn:

(i) Two regions of prolate deformation are found. They occur around $N = 64$ and $N = 102$ with maximum deformation about $\beta \approx 0.30$. The deformation energy (between spherical and deformed shape) is about 6.70 MeV for $N = 64$ and

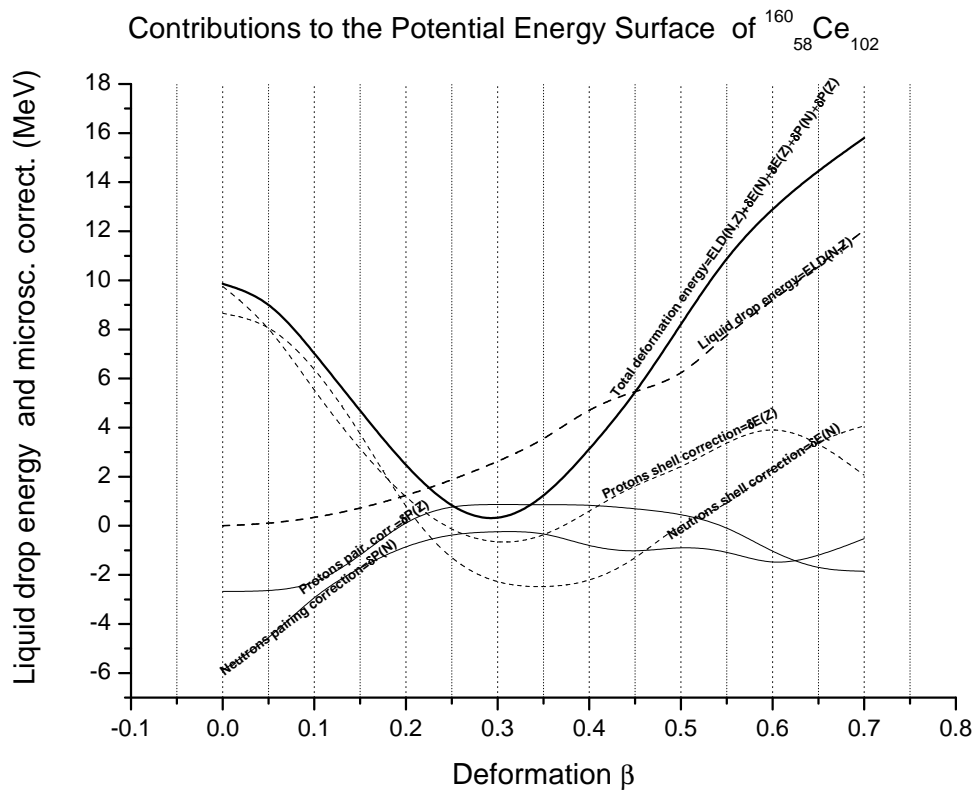


Fig. 1: Contributions of the shell and pairing corrections for the two kind of nucleons and the one of the liquid drop model to the total potential energy surface of the nucleus ^{160}Ce .

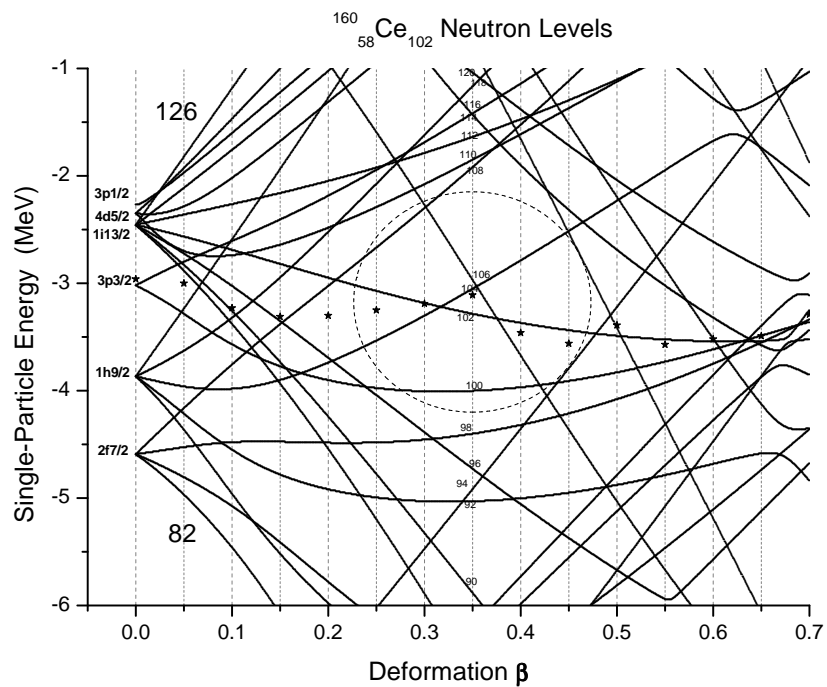


Fig. 2: Single-particle energies of the microscopic model as function of deformation for prolate shapes ($\beta > 0$) for the nucleus ^{160}Ce . Spherical spectroscopic notation is given for spherical deformation ($\beta = 0$). The circle in dotted line indicates the area of lowest level density.

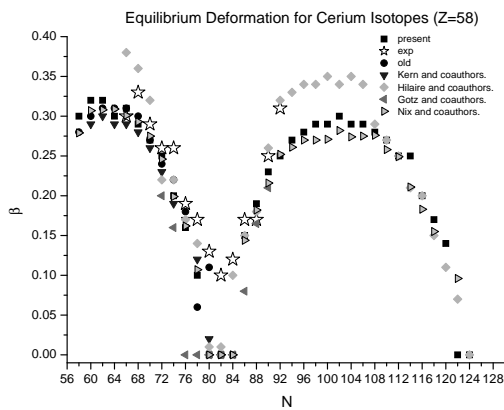


Fig. 3: Theoretical equilibrium deformations for even-even cerium isotopes evaluated by different or similar approaches.

9.30 MeV for $N = 102$ and decreases from either side from these two nuclei.

(ii) Spherical deformation occur at and near the (magic) numbers $N = 82$ and $N = 128$ (not shown).

(iii) The deformation energy decreases from $N = 64$ (maximum) to $N = 82$ (minimum) and reincreases again to $N = 102$ (maximum). We have found graphically that the first inflexion point occurs between $N = 72$ and $N = 74$ and a second inflexion point is found between $N = 90$ and $N = 92$. One can consider (somewhat arbitrarily) that spherical shapes occur approximately between these two limits.

(iv) The minima of prolate equilibrium deformations are, by far, always deeper compared to the ones of the oblate minima ($min_{pro} \ll min_{obl}$). In other words cerium isotopes prefer, by far, prolate shapes. In other words, the deformation energy increases in average with the asymmetry γ . This justifies a posteriori that, in a static study of the equilibrium deformation, it is needless to account for axial asymmetry. It is worth to remember that most of nuclei of the chart have prolate shape (see [25]).

(v) Even though the experimental deformations are known only in absolute value from $B(E2)$, a good agreement is obtained if one excepts the three “nearly magic” nuclei $^{138-142}\text{Ce}$

In Fig. (3) are displayed the present equilibrium deformations, experimental values [1], our “old” calculations [7] and other studies performed by different authors which are: Kern et al. [32], Hilaire and Girod [34], Gotz et al. [33] and Nix et al. [18]. All calculations are based on Macro-Micro method (with different mean fields or different parameters). Except the one of [34] which uses Hartree-Fock-Bogoliubov model with Gogny force.

(i) Near magic number ($N = 82$) all calculations give spherical equilibrium deformation whereas experimental results are always slightly deformed (even for $N = 82$). It seems difficult to overcome this defect with a pure static approach which neglects the role of the mass parameters.

(ii) The overall tendency of these calculations is the same except the fact that HFB calculations differ significantly from the others with higher values in some regions.

(iii) Apart from HFB calculations, theoretical values are generally quite close from each others.

(iv) Our old and new calculations give very close results (see Table 3). Thus, even if it is better to choose a proper set of mean-field parameters for each nucleus, we do not commit a significant error by taking the same set of parameters for nuclei that do not differ strongly by the number of neutrons (N).

3.3 Mass excesses

We list from a FORTRAN file (see Fig. 4) the results of our theoretical calculations of the binding energies and mass excesses (m-excess) for the even-even cerium isotopic chain. For the sake of completeness, experimental mass excesses and the ones of the FRDM model (see [18]) are also given. We must keep in mind that only 6 parameters are used in the liquid drop model whereas 16 parameters are necessary in the FRDM model. This explains the “better quality” of the FRDM model. However, we have checked that the variations of binding energy or mass excesses from one isotope to the nearest is practically the same in our model and the one of FRDM (the deviations are about ± 0.35 MeV). For this reason, the calculation of the two neutron separation energies (see the following subsection 3.4) will almost be probably the same for the two approaches even though our model is not so accurate.

3.4 Transitional regions in cerium isotopes

In Fig. 5 is shown the gradual transition in the potential energy surface from spherical vibrator to the axially deformed rotor when the number of neutrons (N) increases from 76 to 92. One signature of $X(5)$ symmetry which is a critical-point of phase/shape transitions (quantum phase transition between spherical and axial symmetries) should be a long flatness of the potential energy surface with eventually a weak barrier from prolate to oblate shapes. In this figure, for $N > 82$, the width of the flatness increases as one moves away from $N = 82$ but at the same time the difference between oblate and prolate minima and barrier between oblate and prolate shapes also increase. For example the differences between oblate and prolate energy minima and barriers for isotopes with $N = 88, 90, 92$ are respectively about 1.5 MeV, 2.5 MeV and 3.3 MeV with energy barrier about 2 MeV, 4 MeV and 5.5 MeV respectively. The wideness of the bottom of the well must be relativized with the height of the barrier. Thus for the case of $N = 92$ the width is important, i.e. about $\Delta\beta \approx \beta_{pro} - \beta_{obl} \approx 0.26 - (-0.20) \approx 0.46$ but the barrier is about 5.5 MeV and therefore seems too high. The case $N = 90$ gives a width of $\Delta\beta \approx 0.3$ with a barrier of about 4 MeV. For $N < 82$, the case $N = 76$ seems to be rela-

N	A	β_{pro}	$minpro$ (MeV)	β_{obl}	$minobl$ (MeV)	E_{def} (MeV)	$ \beta_{exp} $	N	A	β_{pro}	$minpro$ (MeV)	β_{obl}	$minobl$ (MeV)	E_{def} (MeV)	$ \beta_{exp} $
58	116	0.30	0.90	-0.21	3.62	4.80		92	150	0.25	1.23	-0.17	4.45	5.12	0.31
60	118	0.32	0.88	-0.23	4.07	5.87		94	152	0.27	1.21	-0.19	5.05	6.40	
62	120	0.32	1.03	-0.23	4.33	6.19		96	154	0.28	0.64	-0.21	4.94	7.47	
64	122	0.31	1.16	-0.23	4.23	6.68		98	156	0.29	0.66	-0.22	5.13	8.44	
66	124	0.30	1.47	-0.21	4.15	6.17	0.30	100	158	0.29	0.71	-0.22	5.14	9.08	
68	126	0.29	1.75	-0.21	3.87	5.43	0.33	102	160	0.30	0.32	-0.22	4.52	9.27	
70	128	0.27	1.82	-0.21	3.48	4.67	0.29	104	162	0.29	0.71	-0.22	4.42	9.08	
72	130	0.25	2.02	-0.2	3.27	3.34	0.26	106	164	0.29	1.00	-0.23	4.23	8.44	
74	132	0.20	1.90	-0.17	2.60	1.97	0.26	108	166	0.28	1.16	-0.23	3.92	7.57	
76	134	0.16	1.28	-0.14	1.63	0.93	0.19	110	168	0.27	1.46	-0.21	3.84	6.39	
78	136	0.10	0.04	-0.07	0.18	0.19	0.17	112	170	0.25	1.68	-0.20	3.55	5.33	
80	138	0.00	-1.93	0.00	-1.93	0.00	0.13	114	172	0.25	1.97	-0.19	3.20	4.19	
82	140	0.00	-3.96	0.00	-3.96	0.00	0.10	116	174	0.2	1.93	-0.17	2.79	2.95	
84	142	0.00	-2.07	0.00	-2.07	0.00	0.12	118	176	0.17	1.71	-0.16	2.17	1.68	
86	144	0.15	0.02	-0.06	0.53	0.50	0.17	120	178	0.14	1.39	-0.14	1.60	0.55	
88	146	0.19	0.73	-0.11	2.43	1.99	0.17	122	180	0.0	0.3	0.00	0.30	-0.15	
90	148	0.23	1.15	-0.14	3.76	3.15	0.25	124	182	0.0	-1.08	0.00	-1.08	-0.08	

Table 2: Equilibrium deformations as well as deformation energies for the cerium isotopic chain. The columns give successively the number of neutrons (N), the mass number (A), the prolate equilibrium deformation (β_{pro}), the minimum of the prolate well ($minpro$), the oblate equilibrium deformation (β_{obl}), the minimum of the oblate well ($minobl$), the deformation energy (E_{def} , see text), the experimental equilibrium deformation (β_{exp}). Note: The deformation energy is always given for the prolate equilibrium shape because no absolute minimum is obtained for oblate shape.

Cerium ($Z = 58$)	$N = 58$	60	62	64	66	68	70	72	74	76	78	80	82
Present β	+0.30	+0.32	+0.32	+0.31	+0.30	+0.29	+0.27	+0.25	+0.20	+0.16	+0.10	+0.00	+0.00
Old β	+0.28	+0.30	+0.31	+0.31	+0.31	+0.30	+0.27	+0.24	+0.22	+0.18	+0.06	+0.11	+0.00
Present $E_{def}(MeV)$	4.80	5.87	6.19	6.68	6.17	5.43	4.67	3.34	1.97	0.93	0.19	0.00	0.00
Old $E_{def}(MeV)$	4.82	5.77	6.03	6.31	7.08	5.36	4.41	3.35	2.13	0.77	0.00	0.24	0.00

Table 3: New equilibrium deformations and deformations energies vs old [7].

tively equivalent to $N = 90$ with a slightly smaller width and a lower height barrier. Thus it is difficult to determine clearly the existence of a $X(5)$ critical-point. Thus, everything seems to indicate a continuous transition.

In Fig. 6 is displayed the two-neutron separation energy (TSN) as function of the neutron number N . A clear jump is seen from $N = 82$ to $N = 84$, i.e. from one major shell to the following. Just before $N = 82$ and just after $N = 84$ the TSN varies more slowly. Far for the “jump” the curve becomes quasi-linear. Once again, no special behavior is noted around $N = 90$ which from [35] and [36] should constitute with $Z \approx 62$ the first order shape transition ($X(5)$ critical-point) in the rare earth region. In [37], it has been pointed out that “Empirical evidence of transitional symmetry at the $X(5)$ critical-point has been observed in ^{150}Nd , ^{152}Sm , ^{154}Gd , and ^{156}Dy ”. One of the most important signatures of the phase transition is given by a sudden jump in the value of the energy ratio $R_{4/2} = 4_1^+/2_1^+$ from one nucleus to the next. We found it useful to compare the experimental values of this ratio (see Fig. 7) in the cases of the isotopic chains of Ce and Sm (The experimental values of the considered levels have been deduced from the adopted level of *ENSDF* site [38]). The figure shows clearly two facts. First, the important variation

of $R_{4/2}$ near of the magic number $N = 82$ for both isotopic chains and then, the important difference between the behavior the two isotopic chain from $N = 88$ to $N = 90$. In effect

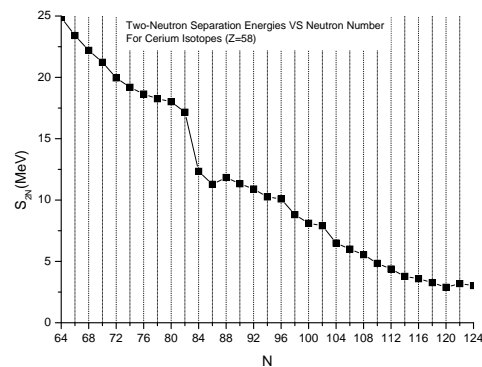


Fig. 6: Two-neutron separation energies (S_{2N}) along the cerium isotopic chain. This quantity is defined as $S_{2N}(A, Z, N) = Bind(A, Z, N) - Bind(A - 2, Z, N - 2)$ where the binding energy $Bind(A, Z, N)$ is given by (1). Note that in our approach the neutron drip line (where $S_{2N} \approx 0$) can be extrapolated around $N = 128$ for Cerium isotopes.

N	58	A	116.	Z	58	bind	914.85	m-excess	-23.94	exp	*****	frdm	-29.21
N	60	A	118.	Z	58	bind	942.64	m-excess	-35.59	exp	*****	frdm	-40.57
N	62	A	120.	Z	58	bind	968.86	m-excess	-45.66	exp	*****	frdm	-50.01
N	64	A	122.	Z	58	bind	993.74	m-excess	-54.40	exp	*****	frdm	-57.99
N	66	A	124.	Z	58	bind	1017.15	m-excess	-61.67	exp	*****	frdm	-64.93
N	68	A	126.	Z	58	bind	1039.35	m-excess	-67.73	exp	*****	frdm	-70.82
N	70	A	128.	Z	58	bind	1060.58	m-excess	-72.81	exp	*****	frdm	-75.54
N	72	A	130.	Z	58	bind	1080.54	m-excess	-76.63	exp	*****	frdm	-79.17
N	74	A	132.	Z	58	bind	1099.73	m-excess	-79.68	exp	*****	frdm	-81.89
N	76	A	134.	Z	58	bind	1118.37	m-excess	-82.18	exp	-84.750	frdm	-84.02
N	78	A	136.	Z	58	bind	1136.63	m-excess	-84.30	exp	-86.500	frdm	-85.67
N	80	A	138.	Z	58	bind	1154.66	m-excess	-86.18	exp	-87.570	frdm	-87.62
N	82	A	140.	Z	58	bind	1171.81	m-excess	-87.19	exp	-88.090	frdm	-88.68
N	84	A	142.	Z	58	bind	1184.16	m-excess	-83.39	exp	-84.540	frdm	-84.78
N	86	A	144.	Z	58	bind	1195.44	m-excess	-78.53	exp	-80.440	frdm	-80.23
N	88	A	146.	Z	58	bind	1207.28	m-excess	-74.23	exp	-75.720	frdm	-76.00
N	90	A	148.	Z	58	bind	1218.60	m-excess	-69.41	exp	-70.430	frdm	-70.83
N	92	A	150.	Z	58	bind	1229.50	m-excess	-64.17	exp	-64.990	frdm	-65.80
N	94	A	152.	Z	58	bind	1239.76	m-excess	-58.28	exp	*****	frdm	-59.78
N	96	A	154.	Z	58	bind	1249.85	m-excess	-52.23	exp	*****	frdm	-52.90
N	98	A	156.	Z	58	bind	1258.66	m-excess	-44.90	exp	*****	frdm	-45.40
N	100	A	158.	Z	58	bind	1266.78	m-excess	-36.87	exp	*****	frdm	-37.29
N	102	A	160.	Z	58	bind	1274.68	m-excess	-28.63	exp	*****	frdm	-28.70
N	104	A	162.	Z	58	bind	1281.19	m-excess	-19.00	exp	*****	frdm	-19.01
N	106	A	164.	Z	58	bind	1287.19	m-excess	-8.86	exp	*****	frdm	-8.62
N	108	A	166.	Z	58	bind	1292.74	m-excess	1.74	exp	*****	frdm	2.23
N	110	A	168.	Z	58	bind	1297.58	m-excess	13.04	exp	*****	frdm	13.43
N	112	A	170.	Z	58	bind	1301.96	m-excess	24.81	exp	*****	frdm	25.00
N	114	A	172.	Z	58	bind	1305.73	m-excess	37.17	exp	*****	frdm	36.82
N	116	A	174.	Z	58	bind	1309.33	m-excess	49.72	exp	*****	frdm	49.07
N	118	A	176.	Z	58	bind	1312.60	m-excess	62.59	exp	*****	frdm	61.53
N	120	A	178.	Z	58	bind	1315.49	m-excess	75.84	exp	*****	frdm	74.94
N	122	A	180.	Z	58	bind	1318.69	m-excess	88.79	exp	*****	frdm	87.48
N	124	A	182.	Z	58	bind	1321.72	m-excess	101.90	exp	*****	frdm	99.94

Fig. 4: Theoretical binding energies and mass excesses of the present approach compared to the experimental mass excesses and the ones given by the FRDM model of [18]. All energies are expressed in MeV. The experimental data as well as the frdm results have been entered manually in the code. Asterics mean that no experimental data is available for the corresponding nucleus.

in the case of Samarium, there is a sudden increase of this ratio whereas this is not the case for the Cerium isotopes. This has been attributed to the X(5) critical-point symmetry of the nucleus ¹⁵²Sm. Thus the present study confirms that cerium isotopic chain is characterized by a continuous shape/phase

transition.

4 Conclusion

Potential energy surfaces have been drawn for the cerium isotopic chain. All even-even nuclei between the two drip lines have been considered. To this end, we have used the microscopic-macroscopic method in which the quantum corrections have been evaluated by a semi-classical procedure. The microscopic model is based on a “realistic” Schrödinger equation including a mean field of a Woods-Saxon type. The macroscopic part of the energy is evaluated from the liquid drop model using the version of Myers and Swiatecki. The following points must be remembered:

- (i) All equilibrium deformations have been found prolate with an important deformation energy compared to oblate shapes.
- (ii) The maximum deformations are of order $\beta \approx 0.3$ and are located around $N = 64$ and $N = 102$ with deformation energy about 6 MeV and 9 MeV respectively. The equilibrium deformations decrease as one moves away from these two nuclei.
- (iii) Spherical shapes are found in the neighborhood of $N = 82$.
- (iv) Good agreement is obtained between theoretical and experimental values if one excepts the area of the shell closure $N = 82$ where the latter are slightly larger.

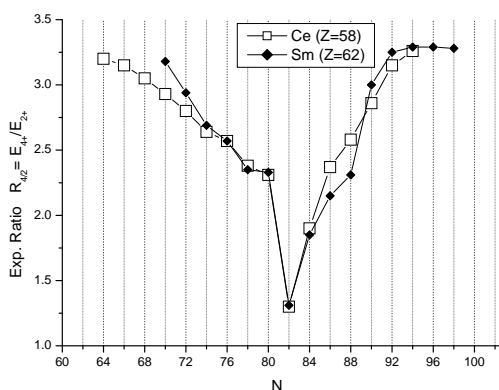


Fig. 7: $R_{4/2}$ energy ratio as function of neutron number for Cerium and Samarium isotopes. Sudden variations are associated with magic closure shells for the both chains (at $N = 82$) and with X(5) critical point which occurs only for Sm (at $N = 90$).

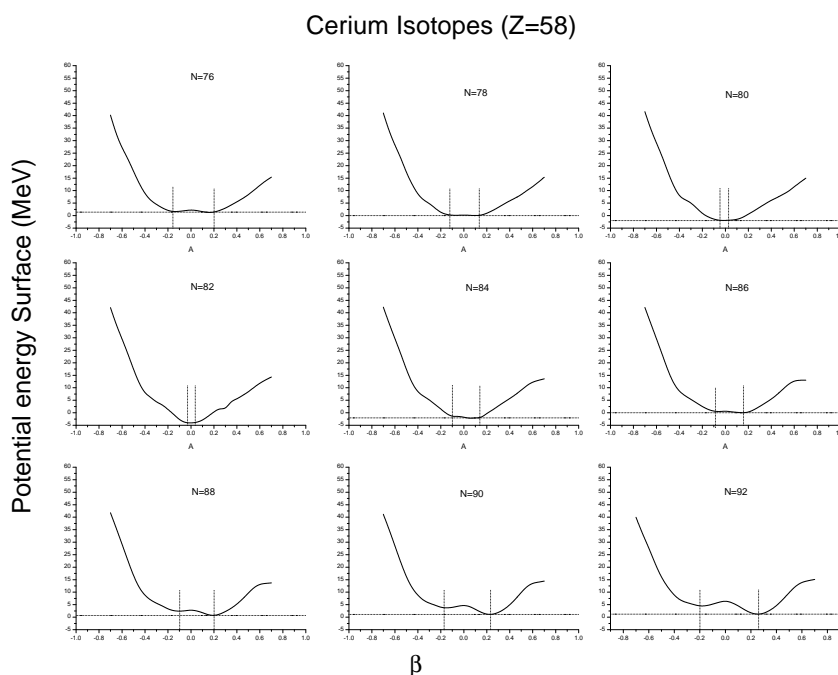


Fig. 5: Shape evolution for cerium isotopes from $N = 78$ to $N = 92$.

(v) This isotopic chain possesses a continuous shape/phase transition from spherical shapes toward the axially symmetric ones.

Submitted on May 2, 2015 / Accepted on May 22, 2015

References

- Raman S., Nestor C. W. Jr. and Tikkanen P. *At. Data Nucl. Data Tables*, 2001, v. 78, 1.
- Stone N. J., *At. Data Nucl. Data Tables*, 2005, v. 90, 75.
- Boboshin I., Ishkhanov B., Komarov S., Orlin V., Peskov N., and Varlamov V. ND 2007 – International Conference on Nuclear Data for Science and Technology. Nice, France, April 22–27 2007.
- Iachello F. and Arima, A. *The Interacting Boson Model*. Cambridge University Press, Cambridge, 1987.
- Bayram T. *Rom. Journ. Phys.*, 2013, v. 58 (7–8), 931–938.
- Bhagwat A., Viñas X., Centelles M., Schuck P., and Wyss R. *Phys. Rev. C*, 2010, v. 81, 044321.
- Mohammed-Azizi B. and Medjadi D. E. *J. Phys. G : Nucl. Part. Phys.*, 2008, v. 35, 035101.
- Cejna P., Jolie J., Casten R. F. *Rev. Mod. Phys.*, 2010, v. 82, 2155–2212.
- Khalaf A. M., Gaballah N., Elgabry M. F. and Ghanim H. A. *Progress in Physics*, 2015, v. 11(2), 141–145.
- Smith J. F. et al. *Phys. Lett.*, 2005, v. B625, 203.
- Todd D. M. et al. *J. Phys. G. Nucl. Phys.*, 1984, v. 10, 1407.
- Kirwan A. J., Ball G. C., Bishop E. J., Godfrey M. J., Nolan P. J., Thornley D. J., Love D. J. G. and Nelson A. H. *Phys. Rev. Lett.*, 1987, v. 58, 467.
- Michelakakis E. et al. 4. International Conference on Nuclei Far From Stability, Helsingør, Denmark, 7–13 Jun 1981. In European Organization for Nuclear Research, Geneva, Switzerland, (20 Jul 1981), pp. 581–588.
- Devi R., Sehgal B. D. and Khosa S. K. *Pramana Journal of Physics*, 2006, v. 67 (3), 467–475.
- Bhat R. K., Devi R., and Khosa S. K. *Brazilian Journal of Physics*, 2003, v. 33 (2), 340–345.
- Long Wen Hui, Ring Peter, Meng Jie, Giai Nguyen Van, and Bertulani Carlos A. *Phys. Rev. C*, 2010, v. 81, 031302.
- Pittel S., Lei Y., Fu G. J. and Zhao Y. M. *Journal of Physics: Conference Series*, 2013, v. 445, 012031.
- Moller P., Nix J. R., Myers W. D. and Swiatecki W. J. *At. Data Nucl. Data Tables*, 1995, v. 59, 185.
- Goriely S., Samyn M., Bender M. and Pearson J. M. *Phys. Rev. C*, 2003, v. 68, 054325.
- Delaroche J.-P., Girod M., Libert J., Goutte H., Hilaire S., Péru S., Pillet N., and Bertsch G. F. *Phys. Rev. C*, 2010, v. 81, 014303.
- Geng L., Toki H. and Meng J. *Progress of Theoretical Physics*, 2005, v. 113 (4), 785–800.
- Mohammed-Azizi B. and Medjadi D. E. *Comput. Phys. Commun.*, 2004, v. 156, 241–282.
- Mohammed-Azizi B. and Medjadi D. E. *Comput. Phys. Commun.*, 2007, v. 176, 634–635.
- Mohammed-Azizi B. and Medjadi D. E. *Comput. Phys. Commun.*, 2014, v. 185, 3067–3068.
- Stránký P., Frank A. and Bijker R. *Journal of Physics: Conference Series*, 2011, v. 322, 012018.
- Mohammed-Azizi B. and Medjadi D. E. *Phys. Rev. C*, 2006, v. 74, 054302.
- Mohammed-Azizi B. *Intern. Journal of Modern Physics C*, 2010, v. 21 (5), 681–694.
- Myers W. D. and Swiatecki W. J. *Nucl. Phys. A*, 1966, v. 81, 1.
- Cwiok S., Dudek J., Nazarewicz W. and Werner T. *Comput. Phys. Commun.*, 1987, v. 46, 379.
- Pauli H. C. *Phys. Lett. C*, 1973, v. 7, 35.

31. Brack M., Damgaard L., Jensen A. S., Pauli H. C., Strutinsky V. M. and Wong C. Y. *Rev. Mod. Phys.*, 1972, v. 44, 320–405.
32. Kern B. D. et al. *Phys. Rev. C*, 1987, v. 36, 1514.
33. Gotz U., Pauli H. C., and Adler K. *Nucl. Phys. A*, 1971, v. 175, 481.
34. Hilaire S., Girod M. http://www-phynu.cea.fr/science_en_ligne/carte_potentiels_microscopiques/carte_potentiel_nucleaire.htm, Jan. 2015.
35. Casten R. F., Cakirli R. B. *Acta Physica Polonica B*, 2009, v. 40 (3), 493–502.
36. Anghel S., Danil G. C., Zamfir N. V., *Romanian Journ. Phys.*, 2009, v. 54 (3–4), 301–319.
37. Sarriguren P., Rodriguez-Guzman R. R., Robledo L. M. *Journal of Physics: Conference Series*, 2010, v. 205, 012024.
38. <http://www.nndc.bnl.gov/ensdf/>, January 2015.

A Constants of the binding energy of the liquid drop model

The constants of (1) are defined as follows:

$$C_V = a_V [1 - \kappa I^2] \quad (\text{in the volume term})$$

$$C_S = a_S [1 - \kappa I^2] \quad (\text{in the surface term})$$

$$I = \frac{N - Z}{N + Z} \quad (\text{relative neutron excess})$$

$$\varepsilon = +1 \quad (\text{even - even}) \quad (\text{in the pairing term}),$$

$$0 \quad (\text{odd}),$$

$$-1 \quad (\text{odd - odd})$$

$$C_C = \frac{3}{5} \frac{e^2}{r_0} \quad (\text{in the Coulomb term})$$

$$C_d = \frac{\pi^2}{2} \left(\frac{a_0}{r_0} \right)^2 \frac{e^2}{r_0} \quad (\text{diffuseness correction})$$

The last correction to the Coulomb energy takes into account that the liquid drop has not a sharp but a diffuse surface of the Woods-Saxon type. The diffuseness parameter is a_0 and the charge radius “contains” r_0 ($R_{ch} = r_0 A^{1/3}$).

B Constants of the Woods-Saxon mean potential

“Universal parameters” of the Woods-Saxon central and Spin-orbit potentials entering in (10).

Neutrons

$$V_{0neut} = 49.6(1 - 0.86I) \quad \text{depth of cmf (MeV)}$$

$$R_{Vneut} = 1.347A^{1/3} \quad \text{radius of cmf (fm)}$$

$$\lambda = 35.0 \quad (\text{dimensionless}) \quad \text{spin-orb. coupling strength}$$

$$R_{SO-neut} = 1.310A^{1/3} \quad \text{Radius of somf (fm)}$$

$$a_0 = 0.70 \quad \text{diffuseness of cmf (fm)}$$

$$a_0 = 0.70 \quad \text{diffuseness of somf (fm)}$$

Protons

$$V_{0prot} = 49.6(1 + 0.86I) \quad \text{depth of cmf (MeV)}$$

$$R_{Vprot} = 1.275A^{1/3} \quad \text{radius of cmf (fm)}$$

$$\lambda = 36.0 \quad (\text{dimensionless}) \quad \text{spin-orb. coupling strength}$$

$$R_{SO-prot} = 1.200A^{1/3} \quad \text{radius of somf (fm)}$$

$$a_0 = 0.70 \quad \text{diffuseness of cmf (fm)}$$

$$a_0 = 0.70 \quad \text{diffuseness of somf (fm)}$$

cmf = central mean field

somf = spin-orbit mean field